CHINESE OPTICS LETTERS

Vol. 21, No. 1 | January 2023

Optical fiber-based magnetically-tuned graphene mechanical resonator

Hongqian Cao (曹鸿谦)[†], Zengyong Liu (刘增勇)[†], Danran Li (李丹然), Zhenda Lu (鲁振达), Ye Chen (陈 烨)[*], and Fei Xu (徐 飞)[**]

College of Engineering and Applied Sciences, Nanjing University, Nanjing 210093, China

[*]Corresponding author: yechen@nju.edu.cn

[**]Corresponding author: feixu@nju.edu.cn

Received March 17, 2022 | Accepted August 4, 2022 | Posted Online August 28, 2022

In this study, an optical fiber-based magnetically-tuned graphene mechanical resonator (GMR) is demonstrated by integrating superparamagnetic iron oxide nanoparticles on the graphene membrane. The resonance frequency shift is achieved by tuning the tension of the graphene membrane with a magnetic field. A resonance frequency tunability of 23 kHz using a 100 mT magnetic field is achieved. The device provides a new way to tune a GMR with a non-contact force. It could also be used for weak magnetic field detection in the future with further improvements in sensitivity.

Keywords: optical fiber; graphene mechanical resonator; magnetically tuned resonator.

DOI: 10.3788/COL202321.010601

1. Introduction

Micro/nanomechanical resonators have attracted considerable attention from scholars in the past decades. Their small size, flexibility, compatibility, high sensitivity, and low power consumption are useful in fundamental researches and applied engineering. They have several applications in mass[1,2], molecules[3], motion and stress[4] detection, metamaterials[5,6], gyroscopes[7], imaging[8], modulators, and sensors[9–11]. Compared with their silicon and silicon-nitride counterparts[12], micro/nanoelectromechanical system (MEMS/NEMS) devices based on thin two-dimensional (2D) material membranes, such as graphene[13–17], MoS_2[18,19], WSe_2[20], and $MoTe_2$[21], take advantage of their thinner dimensions, which make them more compactible. Resonance frequency is the most important factor of mechanical resonators carrying essential information like inner tension and geometric configuration. The graphene sheet-based MEMS was first developed in 2007 by Scott *et al.*[13]. In the paper, the resonance frequencies with different thicknesses and lengths of graphene were studied using the electrical actuation method. Later, abundant studies were conducted benefiting from graphene's easy fabrication (i.e., by chemical vapor deposition, functional nanoparticle decorating), low cost, and robust features. Among them, Chen *et al.* investigated the mechanical performance of monolayer graphene nanomechanical resonators using the electrical readout mechanism[22] in 2009. Barton *et al.* studied the photothermal self-oscillation and laser cooling of a graphene optomechanical resonator in 2012[23]. These studies revealed the frequency shift of resonators changes with several factors, e.g., geometry configuration and inner tension.

The resonance frequency of a graphene mechanical resonator (GMR) can be read out by electrical or optical methods[2,13,23]. In the optical actuation and readout method[23], a Fabry–Pérot (F-P) resonator is formed by the suspended membrane and substrate backplane. The intensity variations of the reflected detection laser reveal the membrane's vibrations, whereby the resonance frequency is analyzed. However, a GMR cannot be actuated or tuned naturally by a magnetic field. The thought of inducing the magnetic response of graphene membranes by external elements works, but few studies have focused on it. One way to achieve this goal is depositing an electrode on graphene to induce a Lorentz force using the current[24]. Another route is to deposit magnetic nanoparticles on graphene. Superparamagnetic iron oxide nanoparticles (SPIONs) are synthesized γ-Fe_2O_3 or Fe_3O_4 particles smaller than 20 nm with an organic or inorganic coating, which own the superiority of no hysteresis compared with traditional magnetic particles. The SPIONs have efficient field strength response and are widely used in biomedical applications such as magnetic resonance imaging[25], cell tracing[26], and drug delivery[27]. In this study, we developed a novel method to tune the GMR resonance frequency with a magmatic field by integrating SPIONs on a graphene membrane with the help of an optical fiber F-P resonator platform. The resonance frequency shift is achieved by tuning the tension of the graphene membrane with a magnetic field. A resonance frequency tunability of 23 kHz using a 100 mT magnetic field is achieved. The device provides a new way to tune a GMR with a non-contact force. It could also be used for weak magnetic field detection in the future with further improvements in sensitivity.

2. Methods and Results

To fabricate a SPIONs-GMR-integrated resonator, a GMR using a previously reported method[24] [Figs. 1(a) and 1(b)] is fabricated firstly. After the cylindrical F-P resonator was fabricated, a piece of rigid central-arched ultraviolet (UV) glue film (about 50 μm × 100 μm) was transferred on top of graphene as a mask to cover the cylindrical air core [Fig. 1(c)]. The sample was then coated with a ~100 nm-thick gold film via magnetron sputtering to rivet the graphene firmly [Fig. 1(d)]. Subsequently, the UV glue film was carefully removed to avoid breaking the graphene membrane. The GMR sample was then immersed in and out of a SPION (with size of ~60 nm for SPION and with Fe_3O_4 particle diameter of ~20 nm) solution several times to attach SPIONs to the graphene. Then, the device was dried in a drying chamber for several hours so that the liquid molecules on the external graphene surface evaporated thoroughly [Fig. 1(d)]. Later, the graphene membrane was curved to a double-clamped rectangular shape with a femtosecond laser [Fig. 1(f)]. Finally, the optical fiber-based device was encapsulated in a glass tube under vacuum conditions of $\sim 10^{-3}$ Pa. Figure 1(g) shows the finally encapsulated product of the SPIONs-integrated GMR under optical microscopy.

The Raman spectrum of the graphene membrane was recorded to estimate thickness before sputtering gold. As indicated by the G and 2D peaks in Fig. 2(a), the graphene membrane consists of multiple layers[28,29]. The appearance of the D band indicates the structural disorder, the edge effects, or the defects in graphene[30]. Thinner and defect-free graphene may benefit device performance. Scanning electron microscopy

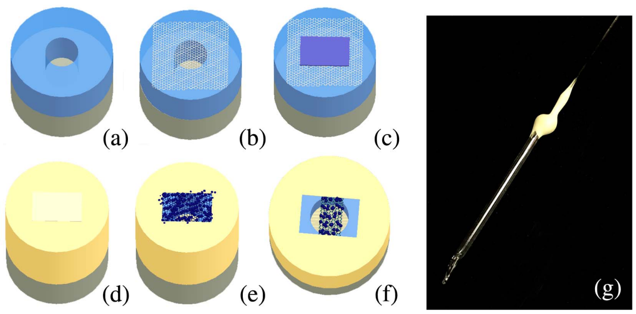

Fig. 1. Process of device fabrication: (a) splicing the capillary glass tube (light blue) with the single-mode optical fiber (gray) and cutting it to a predetermined length (~50 μm); (b) transferring the graphene membrane; (c) covering the air core of the capillary glass tube with UV glue film; (d) riveting the graphene with a ~100-nm-thick gold film coating via magnetron sputtering; (e) removing the UV glue film and attaching the SPIONs onto the graphene; (f) cutting the integrated SPIONs-graphene sheet in a rectangular shape via a femtosecond laser; (g) optical microscopy image of the SPIONs-integrated magnetic field fiber-tuned GMR encapsulated in a glass tube.

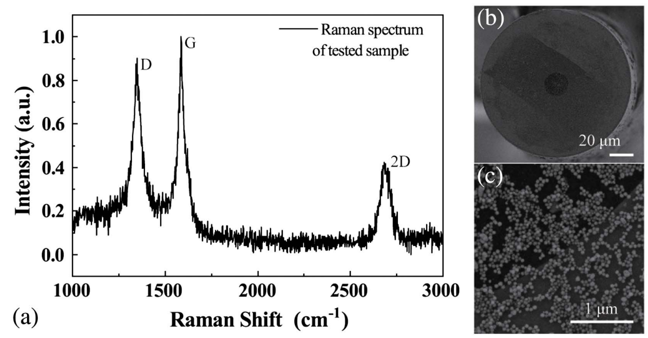

Fig. 2. Characterization of integrated sheet. (a) Raman spectrum of the graphene membrane; (b) SEM image of the graphene membrane; (c) the magnification of (b) to show nanoparticles.

(SEM) images of SPIONs are shown in Figs. 2(b) and 2(c), indicating that the SPIONs were distributed by a single layer, which facilitated the base of the sensing application and ensured a uniform force.

As shown in Fig. 3, the reflected-interference spectrum of the F-P resonator was measured using a broadband optical source and an optical spectrum analyzer (Yokogawa 6370C) before the test. A quadrature point is shown at the spectrum near the wavelength of 1560 nm. The relationship between wavelength shift and power intensity variation is almost linear in the green part.

Figure 4 shows a schematic of the optical actuation and readout setups. Two continuous-wave (CW) lasers are used. One is to actuate (the upper branch), and the other is to detect (the lower branch). A vector network analyzer (VNA, Keysight-N5072) modulates the actuation light (narrow-linewidth fiber laser, SANTEC TSL-700) periodically with sweeping frequencies via an intensity electro-optical modulator (Thorlabs-LN82S-FC) to impose periodic thermoelastic excitation on the suspended integrated graphene sheet. The integrated graphene sheet starts to vibrate with periodic heat absorption (~2.3% absorptivity for graphene), and the motion amplitude reaches the maximum when the modulation frequency matches the resonance frequency.

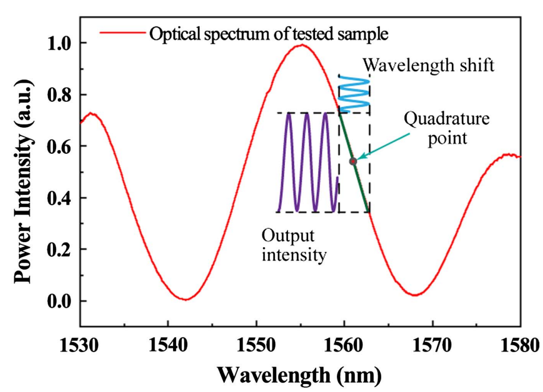

Fig. 3. Optical reflected-interference spectrum of the F-P resonator.

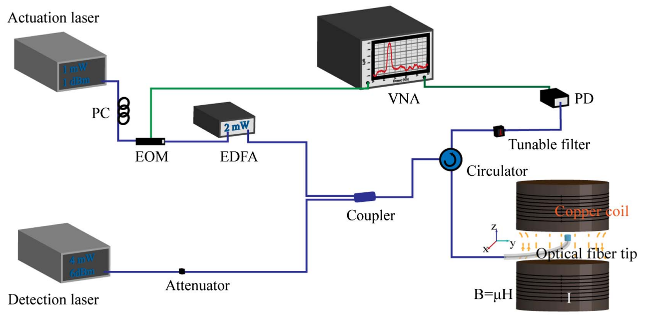

Fig. 4. Schematic of the experimental setup. PC, polarization controller; EOM, electro-optical modulator; EDFA, erbium-doped fiber amplifier; VNA, vector network analyzer; PD, photodetector.

Another narrow-linewidth fiber tunable laser (Agilent-81980A) at the quadrature point provides the detection light, which characterizes the motion of the integrated sheet according to the interference-spectrum shift of the F-P resonator. When the integrated sheet motion occurs with sweeping actuation frequency, the F-P resonator length changes periodically; thus, the interference spectrum shifts (inset illustration in Fig. 3) synchronously. When setting the detection-laser wavelength in the linear region of the F-P spectrum (always the quadrature point), the resonator length change can be read out according to the power intensity variations.

Two lights reach the fiber sample through a circulator after a fiber coupler. The lights interfere when reflected from the SPIONs-integrated graphene and fiber-air interface. A tunable bandpass filter is used to eliminate the reflection of actuation light. Then, the reflected detection light enters a photodetector (PD) and is converted to an electrical signal. Finally, the $|S_{21}|$ factor ($|S_{21}| = \frac{P_{\text{in}}}{P_{\text{out}}}$), i.e., the ratio of the PD signal amplitude to the VNA output modulation power, is used to relatively determine the vibration amplitude. The vibration frequency spectrum is obtained, where maximum vibration amplitude occurs when harmonic resonance happens. As shown in Fig. 5(a), the resonance frequency spectrum is shown in a Lorentzian line shape. The resonance frequency of the tested sample in our experiment was 724.94 kHz. A Cartesian coordinate system can be set with the z axis in the direction of the magnetic field and the x–y plane perpendicular to it. Place the sample in the direction of the integrated sheet in the x–y plane so that the magnetic field changes graphene tension by force applied to SPIONs. Then, the resonance frequency changes with different forces.

The resonance frequency of the graphene membrane is expressed as[31]

$$f = \frac{A}{L}\sqrt{\frac{Et^2}{\rho L^2} + \frac{0.57S}{\rho t}}, \tag{1}$$

where factor A equals 1.03 for a doubly clamped sheet, S represents the tension per width of the sheet, and L, t, ρ, E represent the length, thickness, mass density, and Young's modulus of the membrane, respectively. For a pure graphene membrane with a thickness of 1.07 nm (three layers) and $A = 1.03$, $L = 20\,\mu\text{m}$, $E = 1\,\text{TPa}$, $S = 0.015\,\text{N/m}$, $t = 1\,\text{nm}$, and $\rho = 2200\,\text{kg/m}^3$, the frequency should be 3.10 MHz. Surely, the mechanical parameters of the integrated sheet differed much from pure graphene membrane. Imagine a hybrid sheet made up of nanoparticles and graphene, taking the mass density and Young's modulus of the SPIONs from Refs. [32,33] ($E = 10\,\text{GPa}$, $\rho = 1089\,\text{kg/m}^3$), taking thickness as $t = 60\,\text{nm}$ from Fig. 2(c) to estimate the hybrid sheet's resonance frequency. If the tension of the SPIONs-graphene integrated sheet is adjusted to 0.01318, the frequency would be modified to 725 kHz and 0.01471 to 748.0 kHz of the maximum field. The attachment of SPIONs to graphene changed the effective density, tension, and Young's modulus.

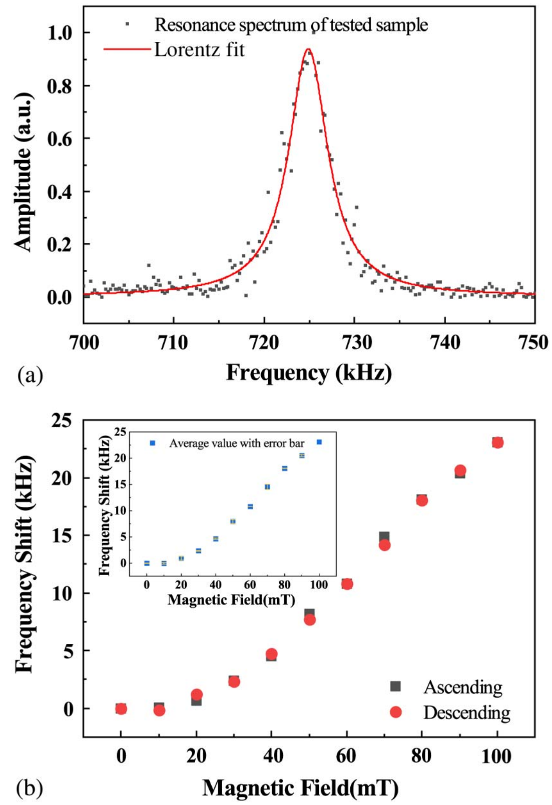

Fig. 5. (a) Resonance frequency spectrum of graphene mechanical resonator; (b) magnetic-field response in the ascending and descending processes. The inset in (b) shows the average value and error bar.

In the experiment, the integrated sheet surface was set perpendicular to the magnetic field line so that the SPIONs maintained balance owing to the force induced by the magnetic field and the supporting force of graphene. Correspondingly, the tension of the graphene changed owing to the counterforce, which led to a variation in the resonance frequency.

As described in Section 2, the Cartesian coordinate system was set with the z axis in the direction of the magnetic field and the x–y plane perpendicular to the integrated sheet. The sheet plane is placed at $z = 0$. The magnetic field generated by concentric circular coils along the z axis exhibited a gradient from $B = 100\,\mathrm{mT}$ at $z = 0$ at the center to $B = 107\,\mathrm{mT}$ at $z \approx 25\,\mathrm{mm}$. However, the field strength was uniform in the center area of the x–y plane in concentric circular coils. The field strength was tuned from 0 to 100 mT and then returned to zero by changing the current in the coil. The repeatability of the ascending and descending processes is shown in Fig. 5(b). When taking a control group with no SPION, the resonance frequency gets no change because of there was no induced magnetic force. Resonance frequency could be tuned by approximately 23 kHz. The average value is shown in the inset together with an error bar. The results indicate the reliability and tunability of the SPIONs-integrated GMR.

3. Discussion

The magnetic-field-induced force of SPIONs is related to the gradient of the field potential energy as follows: $\boldsymbol{F} = -\nabla \boldsymbol{U} = -\nabla(\boldsymbol{m} \cdot \boldsymbol{B})$, where $\boldsymbol{m}$ and $\boldsymbol{B}$ represent the magnetic moment and magnetic field strength, respectively.

The magnetic-field-induced force acting on the SPIONs can be expressed as follows[32]:

$$\boldsymbol{F} = \nabla(\boldsymbol{m}_{\mathrm{NP}} \cdot \boldsymbol{B}) = \rho V(\boldsymbol{M}_0 \cdot \nabla)\boldsymbol{B} + \frac{V\chi_{\mathrm{NP}}}{\mu_0}(\boldsymbol{B} \cdot \nabla)\boldsymbol{B}, \quad (2)$$

where ρ, V, μ_0, χ_{NP}, $\boldsymbol{M}_0$ represent the density, volume, vacuum permeability, magnetic susceptibility (dimensionless), and initial magnetization of the SPIONs, respectively. From Eq. (2), since μ_0, χ_{NP}, $\boldsymbol{M}_0$, V are all constant, the force applied to the SPIONs is determined by the position-related function of the magnetic field $\boldsymbol{B}$.

The relationship between the frequency shift and field strength exhibits a polynomial trend in Fig. 5(b). Because the fiber facet (together with the sheet plane) was set in the x–y plane at $z = 0$, the force on the SPIONs along the z axis is determined by $\boldsymbol{B}(z)$ and $\frac{\partial \boldsymbol{B}(z)}{\partial z}$, which explains the polynomial relationships.

When subjected to the force by the magnetic field, the integrated sheet gets a deformation, which affects the F-P resonator length and induces tension in the sheet. The resonator-length-change-induced wavelength shift or intensity change is relatively tiny to be measured, which requires a high-resolution optical spectrum analyzer. On the other hand, the resonance-frequency-shift method shows the advantage of noticeable sensitivity by tension variation. The resonance frequency-shift method has an enormous potential for applications in microelement measurements and precise analysis.

There are several outlooks. First, the device's sensitivity could be improved by the method of designing the sheet by its morphology or thickness[34] to get a higher tension change by the same field strength variation and lower kinetic energy dissipation. Secondly, the device could also be tuned or driven by an AC magnetic field, which paves the way for magnetically-actuated MEMS devices or sensing applications.

4. Conclusion

We present a new type of SPIONs-integrated GMR based on an optical fiber system, which can be tuned by a magnetic field and read out using an optical method. The integration of those two nanomaterials makes the device combine the advantages of graphene's light weight and small size as a resonator with the SPIONs' hysteresis-free response of magnetic particles to magnetic fields. The proposed device provides a new method for tuning and driving a mechanical resonator with a magnetic field. The resonance frequency tunability of 23 kHz using a 100 mT magnetic field is achieved. It exhibited stable performance as well as good repeatability. This device can be used in complex electrical-interference environments with small working spaces. It is also suitable for situations where heat accumulation (e.g., electrical joule heat) should be avoided. The tunability of the time-varying magnetic field could be verified in the future. With further improvements in the resonator vibration performance, the device can achieve a sensitive response and be used for future weak magnetic field detection or magnetic-field-related applications.

Acknowledgement

This work was supported by the National Natural Science Foundation of China (Nos. 62005118 and 62035006).

References

1. K. L. Ekinci, X. M. H. Huang, and M. L. Roukes, "Ultrasensitive nanoelectromechanical mass detection," Appl. Phys. Lett. **84**, 4469 (2004).
2. M. Muruganathan, H. Miyashita, J. Kulothungan, M. E. Schmidt, and H. Mizuta, "Zeptogram level mass sensing of light weight gas molecules using graphene nanomechanical (GNEM) resonator," in *IEEE Sensors* (2018), p. 1.
3. K. Eom, H. S. Park, D. S. Yoon, and T. Kwon, "Nanomechanical resonators and their applications in biological/chemical detection: nanomechanics principles," Phys. Rep. **503**, 115 (2011).
4. A. Reserbat-Plantey, L. Marty, O. Arcizet, N. Bendiab, and V. Bouchiat, "A local optical probe for measuring motion and stress in a nanoelectromechanical system," Nat. Nanotechnol. **7**, 151 (2012).
5. Z. Ren, Y. Chang, Y. Ma, K. Shih, B. Dong, and C. Lee, "Leveraging of MEMS technologies for optical metamaterials applications," Adv. Opt. Mater. **8**, 1900653 (2019).
6. Y. Chang, J. Wei, and C. Lee, "Metamaterials - from fundamentals and MEMS tuning mechanisms to applications," Nanophotonics **9**, 3049 (2020).
7. Y. Wang, R. Cao, C. Li, and R. N. Dean, "Concepts, roadmaps and challenges of ovenized MEMS gyroscopes: a review," IEEE Sens. J. **21**, 92 (2021).
8. G. C. Zhou, Z. H. Lim, Y. Qi, and G. Y. Zhou, "Single-pixel MEMS imaging systems," Micromachines **11**, 219 (2020).
9. Y. Xu, Z. Lin, X. Huang, Y. Wang, Y. Huang, and X. Duan, "Functionalized graphene hydrogel-based high-performance supercapacitors," Adv. Mater. **25**, 5779 (2013).
10. P. A. Thomas, O. P. Marshall, F. J. Rodriguez, G. H. Auton, V. G. Kravets, D. Kundys, Y. Su, and A. N. Grigorenko, "Nanomechanical electro-optical modulator based on atomic heterostructures," Nat. Commun. **7**, 13590 (2016).
11. J. X. Zhu, X. M. Liu, Q. F. Shi, T. Y. Y. He, Z. D. Sun, X. G. Guo, W. X. Liu, O. Bin Sulaiman, B. W. Dong, and C. Lee, "Development trends and perspectives of future sensors and MEMS/NEMS," Micromachines **11**, 7 (2020).
12. B. Ilic, S. Krylov, K. Aubin, R. Reichenbach, and H. G. Craighead, "Optical excitation of nanoelectromechanical oscillators," Appl. Phys. Lett. **86**, 193114 (2005).

13. B. J. Scott, A. M. Van Der Zande, S. S. Verbridge, I. W. Frank, D. M. Tanenbaum, J. M. Parpia, H. G. Craighead, and P. L. Mceuen, "Electromechanical resonators from graphene sheets," Science **315**, 954 (2007).
14. A. M. Van Der Zande, R. A. Barton, J. S. Alden, C. S. Ruiz-Vargas, W. S. Whitney, P. H. Q. Pham, J. Park, J. M. Parpia, H. G. Craighead, and P. L. McEuen, "Large-scale arrays of single-layer graphene resonators," Nano Lett. **10**, 4869 (2010).
15. Y. Oshidari, T. Hatakeyama, R. Kometani, S. I. Warisawa, and S. Ishihara, "High quality factor graphene resonator fabrication using resist shrinkage-induced strain," Appl. Phys. Express **5**, 117201 (2012).
16. G. J. Verbiest, J. N. Kirchhof, J. Sonntag, M. Goldsche, T. Khodkov, and C. Stampfer, "Detecting ultrasound vibrations with graphene resonators," Nano Lett. **18**, 5132 (2018).
17. Y. Xiao, F. Hu, M. Zhu, J. Zheng, X. Song, Y. Liu, and S. Qin, "Effect of induced current loss on quality factor of graphene resonators," AIP Adv. **12**, 035041 (2022).
18. J. Lee, Z. Wang, and X. L. Feng, "Frequency scaling of molybdenum disulfide (MoS_2) two-dimensional (2D) nanomechanical resonators," in *European Frequency & Time Forum & International Frequency Control Symposium* (2013), p. 58.
19. J. Lee, Z. Wang, K. He, J. Shan, and P. X. L. Feng, "Air damping of atomically thin MoS_2 nanomechanical resonators," Appl. Phys. Lett. **105**, 023104 (2014).
20. N. Morell, A. Reserbat-Plantey, I. Tsioutsios, K. G. Schädler, F. Dubin, F. H. L. Koppens, and A. Bachtold, "High quality factor mechanical resonators based on WSe_2 monolayers," Nano Lett. **16**, 5102 (2016).
21. X. Liu, A. Islam, and P. X. Feng, "Few-layer $MoTe_2$ suspended channel transistors and nanoelectromechanical resonators," in *20th International Conference on Solid-State Sensors, Actuators and Microsystems & Eurosensors XXXIII (Transducers & Eurosensors XXXIII)* (2019), p. 2408.
22. C. Chen, S. Rosenblatt, K. I. Bolotin, W. Kalb, P. Kim, I. Kymissis, H. L. Stormer, T. F. Heinz, and J. Hone, "Performance of monolayer graphene nanomechanical resonators with electrical readout," Nat. Nanotechnol. **4**, 861 (2009).
23. R. A. Barton, I. R. Storch, V. P. Adiga, R. Sakakibara, B. R. Cipriany, B. Ilic, S. P. Wang, P. Ong, P. L. McEuen, J. M. Parpia, and H. G. Craighead, "Photothermal self-oscillation and laser cooling of graphene optomechanical systems," Nano Lett. **12**, 4681 (2012).
24. Z. Liu, H. Cao, and F. Xu, "Fiber-optic Lorentz force magnetometer based on a gold-graphene composite membrane," Appl. Phys. Lett. **112**, 203504 (2018).
25. A. Alipour, Z. Soran-Erdem, M. Utkur, V. K. Sharma, O. Algin, E. U. Saritas, and H. V. Demir, "A new class of cubic SPIONs as a dual-mode T1 and T2 contrast agent for MRI," Magn. Reson. Imaging **49**, 16 (2018).
26. M. Barrow, A. Taylor, J. García Carrión, P. Mandal, B. K. Park, H. Poptani, P. Murray, M. J. Rosseinsky, and D. J. Adams, "Co-precipitation of DEAE-dextran coated SPIONs: how synthesis conditions affect particle properties, stem cell labelling and MR contrast," Contrast Media Mol. Imaging **11**, 362 (2016).
27. E. Jamal Al Dine, Z. Ferjaoui, J. Ghanbaja, T. Roques-Carmes, A. Meftah, T. Hamieh, J. Toufaily, R. Schneider, S. Marchal, E. Gaffet, and H. Alem, "Thermo-responsive magnetic Fe_3O_4@P(MEO2MA$_X$-OEGMA$_{100-X}$) NPs and their applications as drug delivery systems," Int. J. Pharm. **532**, 738 (2017).
28. Z. H. Ni, H. M. Wang, J. Kasim, H. M. Fan, T. Yu, Y. H. Wu, Y. P. Feng, and Z. X. Shen, "Graphene thickness determination using reflection and contrast spectroscopy," Nano Lett. **7**, 2758 (2007).
29. M. Kim, X. Xu, R. Xin, J. Earnshaw, A. Ashok, J. Kim, T. Park, A. K. Nanjundan, W. A. El-Said, J. W. Yi, J. Na, and Y. Yamauchi, "KOH-activated hollow ZIF-8 derived porous carbon: nanoarchitectured control for upgraded capacitive deionization and supercapacitor," ACS Appl. Mater. Interfaces **13**, 52034 (2021).
30. M. A. Pimenta, G. Dresselhaus, M. S. Dresselhaus, L. G. Cancado, A. Jorio, and R. Saito, "Studying disorder in graphite-based systems by Raman spectroscopy," Phys. Chem. Chem. Phys. **9**, 1276 (2007).
31. J. S. Bunch, *Mechanical and Electrical Properties of Graphene Sheets* (Cornell University, 2008).
32. S. S. Shevkoplyas, A. C. Siegel, R. M. Westervelt, M. G. Prentiss, and G. M. Whitesides, "The force acting on a superparamagnetic bead due to an applied magnetic field," Lab Chip **7**, 1294 (2007).
33. H. W. Wang, H. W. Zhou, R. D. Peng, and L. Mishnaevsky, "Nanoreinforced polymer composites: 3D FEM modeling with effective interface concept," Compos. Sci. Technol. **71**, 980 (2011).
34. T. Yang, H. Lin, and B. Jia, "Ultrafast direct laser writing of 2D materials for multifunctional photonics devices [Invited]," Chin. Opt. Lett. **18**, 023601 (2020).